PROCEEDINGS, 48th Workshop on Geothermal Reservoir Engineering
Stanford University, Stanford, California, February 6-8, 2023
SGP-TR-224

Distribution, isotopic composition, and origin of Li in the Salton Sea Geothermal Field

J. Humphreys[1], M. Brounce[1], M. A. McKibben[1], P. Dobson[2], N. Planavsky[3], H.R. Hoover[1], B. Wenzel[1]

[1]University of California Riverside, Riverside CA 92592; [2]Lawrence Berkeley National Laboratory, Berkeley, CA 94720; [3]Yale University, New Haven, CT 06518

Jhump004@ucr.edu

Keywords: Salton Sea Geothermal Field, lithium, mineralogy, metasedimentary, chlorite

ABSTRACT

Hypersaline brines from the Salton Sea Geothermal Field (SSGF) comprise what may be potentially one of the largest known brine deposits of lithium in the world, containing between 1 and 5 million metric tons of dissolved Li metal. With rising global and domestic demand for lithium due to the manufacture of batteries for electric vehicles and other energy storage applications, there is increasing interest in extracting lithium from geothermal brines such as those found in the SSGF. This type of lithium resource is also of interest because it has a relatively small footprint on the surface of the Earth, and thus may have substantially lower environmental impacts when compared to more traditional forms of lithium extraction, such as open pit hard rock mines and evaporative ponds (i.e., salars). In the case of the SSGF brines, it is unclear the extent to which reinjected brines, once lithium has been extracted from them at the surface, might reacquire additional lithium upon interaction with their source rocks at depth, and thus the maximum size of the recoverable resource may exceed that currently found dissolved in the brines.

This study uses petrography, microscopy, Li isotopes, and micro-analytical techniques to identify the sources of lithium in the SSGF brines and rocks, including the dominant mineral hosts of lithium within the host reservoir rocks.

The stratigraphy of the SSGF reservoir consists of metamorphosed Plio-Pleistocene sedimentary rocks (sandstones, mudstones, and evaporites), with intervals of buried rhyolite domes and tuffs and intruded basaltic and rhyolitic dikes (e.g., Herzig et al., 1988; Hulen et al., 2002). Preliminary analyses of polished sections of reservoir rock minerals using laser ablation induced coupled plasma mass spectrometry yield Li concentrations as high as 91 ppm in rhyolite matrix glass and 581 ppm in authigenic (hydrothermal) chlorite. The lowest lithium abundances are measured in epidote, alkali feldspars, pyrite and anhydrite. Groundmass (comprised predominantly of granular biotite and sodic feldspar) concentrations of Li in rocks with these major mineral phases are as low as 12 ppm. When the groundmass contains granular chlorite, groundmass Li concentrations reach as high as 252 ppm, even when chlorite is also present as a major (i.e., >30 μm in diameter) mineral. Chlorite is observed to encase pyrite in anhydrite-bearing rocks, indicating a mineral reaction important to fixing Li in the rocks; this chlorite contains 581 ppm Li - the highest measured Li contents in this study for a single mineral grain. Unaltered surface Holocene rhyolite glasses record Li concentrations up to 91 ppm while their buried late Pleistocene counterparts record Li concentrations of up to 68 ppm.

Fresh surface rhyolites show a wide δ^7Li variation from 3.5 to 10.3 ‰, while older buried, altered intrusive and extrusive rhyolites exhibit a tight δ^7Li clustering from 6.4 to 7.6‰. Metasediment δ^7Li values range from 1.8 to 7.8‰. Li isotopic compositions of the SSGF reservoir brines are relatively light and narrowly confined (δ^7Li = +3.7 to +4.7‰). This δ^7Li brine composition overlaps with previous measurements of δ^7Li in salar brines from South America (δ^7Li = +3.7 - +12.6‰) and playa sediments from Nevada (δ^7Li = -1 - +8‰), is slightly heavier in δ^7Li composition than those reported for lithium-bearing (168-190 ppm Li) geothermal brines from the Rhine Graben (δ^7Li = +1.0 - +1.7‰), and lighter in δ^7Li composition than oil field related brine water from the Rhine Graben (δ^7Li = 7.0 - 12.6‰, 6.9 – 72.0 ppm) and brines from the Tibetan Plateau (δ^7Li = 9.2 – 32.‰, 14.4 – 408.8 ppm). These values also overlap with many different lithium reservoirs, including upper continental crust (δ^7Li_{avg} = 0.6‰), river waters (δ^7Li = +1 - +44‰), and Mid-Ocean Ridge Basalt (δ^7Li_{avg} = 3.4‰). The multiple overlaps in δ^7Li values between Salton Sea brines and rocks with various Li sources, indicates that contact with sedimentary, metasedimentary, and igneous rocks within the Salton Trough have likely all contributed to the chemical characteristics of the current brine. Quantitative handling of the isotopic data will be used in a future contribution to demonstrate the exact source(s) of Li in the SSGF brines and reservoir rocks.

1. INTRODUCTION

Lithium is a highly versatile element that has made it desirable for a number of applications (e.g., lubricants, ceramics, flux powders). Of particular note in the context of this study is the steadily increasing demand for Li as a component in batteries (Ambrose and Kendall, 2020). With efforts to combat climate change focusing on the utilization of more renewable energy resources and the decarbonization of transportation, the demand for Li-batteries as an efficient means for energy storage has increased, as has the interest in establishing large, reliable domestic sources of lithium ores. Lithium is thus considered a critical mineral by the United States Department of Interior (U.S.G.S., 2022).

Currently, lithium mining, refining, and battery assembly is an environmentally damaging process that requires energy- and water-rich, hazardous mining and processing techniques and long distance, international shipping supply chains (Sun et al., 2017). The largest producers of lithium are Chile (in the Andes Mountains, ~26,000 metric tons) and Australia (~55,000 metric tons) which account for

~80% of global lithium production (Jaskula, 2022). Lithium mining, regardless of the form, requires large amounts of water (Chordia et al., 2022; Liu and Agusdinata, 2020) and the amount of greenhouse gas emissions are dependent on the extraction techniques being used (Kelly et al., 2021). Once mined, the majority of Li is shipped to China to be manufactured into Li-based chemical derivatives that are necessary for production of batteries and other Li-based products (Olivetti et al., 2017; Sun et al., 2017). In 2014, the amount of Li-based chemicals produced by China was ~47 kt LCE (lithium carbonate equivalent) or ~56% of the chemical derivatives produced globally (Sun et al., 2017). Alternatively, mining Li in the SSGF would build upon the pre-existing geothermal energy extraction infrastructure and technology already present in the Field, making the physical footprint for this form of Li-mining far smaller than the traditionally employed methods. Additionally, the Imperial Valley, where the Salton Sea Geothermal Field is located, can potentially host electric car battery manufacturing, which could diminish the amount of energy expended to produce Li-batteries by removing the need to ship the mined lithium elsewhere to be converted into batteries. Together, these two possibilities mean that the SSGF offers a possible solution to the global environmental problem that current lithium mining practices present to the U.S.

Current estimates for the Li reserves in the SSGF (between 1 and 5 million metric tons of Li metal) are based on geothermal brine volumes and do not consider additional resources generated by the subsequent subsurface interaction of the reinjected, Li-depleted brine with the host rocks at depth. This ongoing study will characterize the sources and sinks of lithium within the SSGF, as well as eventually the long-term viability of lithium extraction from this field by quantifying the lithium concentrations in individual minerals within the reservoir rocks and their unaltered equivalents at the surface.

2. GEOLOGIC SETTING

The SSGF is located in the southernmost part of California, 60 km north of the United States-Mexico border, on the southeastern shore of the Salton Sea (fig. 1). The Salton Sea is surrounded by a series of transform faults and pull-apart basins (and is notably where the San Andreas Fault starts) that formed as a consequence of the rifting associated with the opening of the Gulf of California (e.g., Elders et al., 1972; Han et al., 2016). Beginning >100 million years ago and continuously until ~12 million years ago subduction of oceanic crust beneath the North American Plate took place off the coast of Southern California and Northern Mexico (Stock and Hodges, 1989). From ~12 million years ago onwards, subduction in this region has been replaced with strike-slip and extensional motion (Stock and Hodges, 1989).

Figure 1: Map of the Salton Sea using satellite images downloaded from Google Earth on 3 May 2022. A) Regional map showing the location of the Salton Sea in relationship to government borders. B) Inset map from A showing the size of the Salton Sea and bounding of the Salton Sea by mountains to the east and west. C) Inset map from B showing a portion of the SSGF and associated rhyolitic domes. Samples from Obsidian Butte and Rock Hill were analyzed during this study.

Upon the opening of the Gulf of California into western North America by ~6 Ma (Matti et al., 1985), the Colorado River deposited sediments into the Gulf, creating a river delta that isolated the northern part of the rifted opening from the remainder of the Gulf of California around 4 Ma (e.g., Winker and Kidwell, 1986). The Colorado River today predominately drains southwards into the Gulf of California, but historically has been periodically captured and re-routed northwards as a result of flooding and this rerouting has filled the

Salton Trough with sediments, creating multiple repeated evaporative salt lakes in the northern Salton Trough (Tompson, 2016). These ancient lakes are collectively known as Lake Cahuilla, after the people who live in the Salton Trough, and are the origin of the sediments, host rocks, and pore waters which exist at depth beneath the Salton Sea today and are the source of the geothermal brines currently being used to power the SSGF today (Coplen, 1976).

The other important geological characteristic of the geothermal field is the heat source that exists beneath it as a result of extensional spreading in the lower crust and upper mantle (e.g., Elders et al, 1972; Han et al., 2016). Surface expressions of this subsurface heat source can be seen on the south-eastern shore of the Salton Sea, where five rhyolitic eruption sites exist at the shoreline of the Salton Sea (fig. 1C). These volcanic domes are ~2,000-12,000 years old (Wright et al., 2015) and are the most recent occurrence of rhyolitic volcanism in the Salton Trough (Schmitt and Hulen, 2008). Starting at ~1500 m below these rhyolitic domes are a series of buried extrusive and intrusive rhyolites that are ~450,000 years old (Schmitt and Hulen, 2008). The repeated volcanism in this region is a shallow expression of the long-standing nature of deep magmatic activity associated with this extensional plate tectonic related heat source.

The subsurface brines beneath the Salton Sea are separated into two immiscible, density divided and distinct fluids: (1) a cooler, lower salinity (<10 wt% total dissolved solids) fluid on top and (2) a hot, hypersaline (>20% total dissolved solids) brine below (Williams and McKibben, 1989). The interface between the lower salinity fluid and the hypersaline brine approximately follows the depth of the 250°C isotherm of the geothermal field, such that in locations where the 250°C isotherm is shallowest, so too is the depth to the brine interface (Williams and McKibben, 1989). This relationship between the brine boundary layer and the 250°C isotherm connects the existence of this hypersaline (and lithium-bearing) brine to the geothermal heat source in this region (Williams and McKibben, 1989). Previous studies of the SSGF hypersaline brines have found that these brines contain on average ~200 ppm Li (Helgeson, 1968; Maimoni, 1982; McKibben et al., 2021; Skinner et al., 1967; Williams and McKibben, 1989). Additionally, drill cuttings from the Salton Sea Geothermal Field show that the reservoir rocks in this field contains 15 - 80 ppm (average 40 ppm) lithium (McKibben et al., 2021).

3. METHODS

3.1 Sample Description

Samples in this study include igneous and sedimentary surface rocks collected in 2022 for this study, geothermal brines collected from 22 commercial wells in the SSGF in 2022, as well as previously analyzed commercial drill cuttings (Schmitt and Hulen, 2008) and State 2-14 drill core specimens (e.g., Elders and Sass, 1988; Herzig et al., 1988; Herzig and Elders, 1988; McKibben et al., 1988a, 1988b). Igneous surface samples come from Obsidian Butte and Rock Hill (Herzig and Jacobs, 1994; Robinson et al., 1976). Sedimentary samples are from surface exposures of the Durmid Hills sedimentary and evaporitic rocks (Babcock, 1974). Surface samples analyzed in this study include the following:

- Spherulitic obsidian from Obsidian Butte. Spherulites are centered around fine grained, subhedral to anhedral phenocrysts of plagioclase and are composed of radiating, acicular crystals of alkali feldspar and quartz. Sparse, fine grained, subhedral clinopyroxene phenocrysts can be found at the center of spherulites, directly next to the larger plagioclase phenocrysts.
- Medium grey, vesicular, aphanitic to glassy rhyolite from Rock Hill. Sparse amounts of fine grained euhedral-subhedral, plagioclase, clinopyroxene, and Fe-Ti oxide crystals are present within the rhyolite.
- Dark grey, vesicular, glassy rhyolite from Rock Hill. Sparse amounts of fine grained subhedral and rounded plagioclase, clinopyroxene, and Fe-Ti oxide crystals are present within the rhyolite. Vesicles are elongated in one direction.
- Light grey mudstone with minor amounts of fine to medium grained pyrite crystals.
- Grey-ish translucent gypsum with light grey, interbedded mudstone. Gypsum beds range from very fine-grained layers of a few mm in thickness to coarser grained, acicular blocks of about 1 cm in thickness.
- White, cryptocrystalline gypsum.
- Light to medium grey, gypsum-cemented, fine-grained sandstone.

3.2 Sample Preparation

Samples were sawn with a diamond-coated blade and washed in de-ionized water before being sent for commercial preparation as polished thin sections by Burnham Petrographics, LLC. Drill cuttings were mixed with epoxy and mounted within 0.7 cm-round brass spacers cut to be 0.6 cm in length, exposed on one side, polished, and carbon coated for SEM analysis.

3.3 Scanning Electron Microscope

Carbon-coated samples were analyzed at the Brounce Geochemical Laboratory at the University of California, Riverside on a JEOL JCM-7000 NeoScope Benchtop scanning electron microscope using an accelerating voltage of 15 kV. Elemental and back-scattered electron maps of samples were analyzed to identify major mineral phases in the samples in conjunction with visible light petrographic observations for the thin sections analyzed. These analyses were then used to identify target regions for analysis of major and trace element concentrations via laser ablation induced coupled plasma mass spectrometry.

3.4 Laser Ablation Inductively Coupled Mass Spectrometry

Trace element abundances for the samples in this study were analyzed at the Lyons ICP-MS Facility at the University of California, Riverside via LA-ICP-MS using an Agilent Technologies 7900 single quadrupole mass spectrometer that is coupled to a short pulse width coherent 193 nm ArF excimer laser. Samples in this study were analyzed for 59 major, minor, and trace elements, including Li. Spot sizes ranged from 25-30 μm. A repeat rate of 5 Hz and energy on sample surface of 0.040 – 0.052 mJ was used. United States Geological Survey glass standards BIR-1 g, BCR-2 g, and BHVO-2 g and Max Planck Institute glass standards KL2-G, ML3B-G, StHls-G, GOR-128-G, GOR-132-G, ATHO-G, and T1-G were used to create linear calibration curves ($R^2 > 0.999$) for each analytical session (Jochum et al., 2000; Kelley et al., 2003). Counting statistics were examined carefully for each element and those elements that did not return strong signals for the entire length of the ablation period were discarded. For minerals where sulfur and/or carbon was a major elemental constituent (i.e., pyrite, anhydrite, gypsum, and calcite), analyses were normalized to either ^{44}Ca (for anhydrite, gypsum, and calcite) or ^{56}Fe (for pyrite) using an assumed CaO or FeO stochiometric concentration (41.3 wt % CaO for anhydrite, 32.6 wt % CaO for gypsum, 56.0 wt % CaO for calcite, and 59.9 wt % FeO for pyrite). To calculate elemental abundances from the signal for the remainder of the samples analyzed, the calculation of concentration method from Gratuze (1999) was followed.

3.5 Lithium Isotopes

Lithium isotopes for the samples in this study were analyzed at the Geochemistry Center at Yale University via a Thermo Finnigan Neptune Plus ICP-MS using the methods of Kalderon-Asael et al. (2021). For the brines, an aliquot of 1 mL of each sample was dried at 93°C into a pre-acid-cleaned Teflon beaker. The aliquots were subsequently digested with aqua regia (200 microliters of distilled HNO_3 and 600 microliters of distilled HCl), capped and left on a hotplate at 130°C for 48 hours, and dried again. At a second digestion step, 1 mL of distilled HNO_3 and three drops of H_2O_2 were added to each sample, capped and left on a hotplate at 130°C for 48 hours, and dried again. The samples were then redissolved in 10 mL of 6N HCl. Splits were taken for lithium column procedure. The rock samples were digested using the total digest protocol. At the end, the samples were redissolved in 5 mL of 6N HCl. The few evaporitic samples were dissolved in MQ H_2O. Splits were taken for the lithium column procedure.

4. RESULTS

Surface rhyolitic rocks have variable lithium isotopic compositions. Obsidian Butte lithium isotopic compositions (whole rock samples) range from 3.5-3.8‰ while Rock Hill δ^7Li ranges from 8.1-10.3‰. Lithium concentrations within these rocks varies by mineralogy (1-91 ppm) with the highest Li concentrations consistently being recorded in the matrix glass (91.2 $\pm$ 2.3 ppm). Buried rhyolitic rocks consistently have δ^7Li values that range from 6.4-7.6‰ and spot analysis lithium concentrations that range from 2-68 ppm. Due to the hydrothermally altered state of these late Pleistocene subsurface volcanic drill cuttings, no mineralogic comparisons can be made between the different analyzed areas; however, based on the SEM elemental maps, a qualitative assessment of the cuttings show that the more Si-rich regions have higher lithium concentration than relatively Ca- or Na-rich regions.

The Li contents of the Durmid Hills surface sedimentary and evaporitic rocks vary by rock type. The minerals within the sandstone contain low concentrations of lithium (1-7 ppm) and δ^7Li = +5.2‰. The mudstone groundmass of the mudstone rock and mudstone that is interbedded with gypsum has relatively high lithium concentrations (142.1 – 172.6 ppm); these values are slightly higher than the reported Li concentrations (104-136 ppm) measured in the clay-size fraction of near-surface sediments from the Salton Sea (Sturz, 1989). Durmid Hills mudstones have 1.5‰ δ^7Li, interbedded mudstone and gypsum range from 5.5-6.0‰. Lithium contents for the cryptocrystalline gypsum are <1 ppm and have a δ^7Li = -9.1‰. The State 2-14 drillcore metasedimentary mudstones found at depths from ~1290-1430 m have a δ^7Li = 1.8‰ for the mudstone that contained anhydrite veins (~1290 m depth) and 5.7-6.3‰ for the mudstone with hematite veins (~1430 m depth). Vein material was not analyzed for these metasedimentary rocks, and care was taken to only sample the mudstone in these cores.

The variation in Li concentration in the metasedimentary rocks varies with the mineralogy. Chlorites, regardless of depth of host rock, have the highest Li concentrations recorded of all the metasedimentary minerals, with concentrations as high as 581 ppm. Mixed biotite-groundmass and calcite-quartz grains had the next highest Li concentrations, as high as 87 ppm. Alkali feldspars in this study range from 3-19 ppm Li. Other minerals, such as anhydrite, pyrite, epidote, and apatite, had Li compositions that were consistently <1 ppm but occasionally as high as 5 ppm Li. The metasedimentary rocks found at depths between 1800 and 2400 m have δ^7Li compositions that range from 2.0-4.3‰. For metasedimentary rocks deeper than 2500 m, δ^7Li = 6.2-7.9‰ for an epidote-rich metasedimentary rock and +4.3 - +5.1‰ for a metabasalt. Geothermal brines in this study have a narrow range in δ^7Li compositions (δ^7Li = 3.7-4.5‰). This δ^7Li brine composition overlaps with previous measurements δ^7Li in salar brines from the Andes (δ^7Li = +3.7 - +12.6‰; Garcia et al., 2020; Godfrey and Álvarez-Amado, 2020; Godfrey et al., 2013; Munk et al., 2018) and Nevada (δ^7Li = -1 - +8‰; Araoka et al., 2014), slightly heavier in δ^7Li composition than those reported for lithium-bearing (168-190 ppm Li) geothermal brines from the Rhine Graben (δ^7Li = +1.0 - +1.7‰; Sanjuan et al., 2016), and lighter in δ^7Li composition than oil field related brines from the Rhine Graben (δ^7Li = 7.0 - 12.6‰, 6.9 – 72.0 ppm; Sanjuan et al., 2016) and Tibetan Plateau (δ^7Li = 31.3 – 32.‰, 14.4 – 97.5 ppm; He et al., 2020) as well as lighter in δ^7Li composition from non-oil well brines originating from melting snow and rain water (δ^7Li = 31.3 – 32.6‰, 14.4 – 97.5 ppm; He et al., 2020) and ancient brine lake and mountain recharge water (δ^7Li = 9.2 – 21.2‰, 8.7 – 408.8 ppm) in the Tibetan Plateau (He et al., 2020).

5. DISCUSSION

From paleomagnetic, isotopic, and infrared stimulated luminescence dating, the rhyolitic domes at the southeastern shore of the Salton Sea are ~2000-12,000 years old (Schmitt et al., 2019; Wright et al., 2015). The presence of the Bishop Tuff within the stratigraphy of the Durmid Hills constrains the ages of these young sedimentary rocks from a few hundred to over 766 thousand years old (Babcock, 1974;

Merriam and Bischoff, 1975; Sarna-Wojcicki et al., 1984; Mark et al., 2017). Over the course of the past 2000 years, Lake Cahuilla has had at least 7 cycles of flooding and evaporation, with the most recent filling of Lake Cahuilla taking place ~300 years ago (Rockwell et al., 2022). At its highstand, the surface of Lake Cahuilla was ~13 m above sea level, or 83 m above the present-day surface of the Salton Sea (Rockwell et al., 2022). At this elevation, Lake Cahuilla would have fully submerged the rhyolitic domes, which have a maximum height of 40 meters below sea level (Robinson et al., 1976; Wright et al., 2015). Presently, the Durmid Hills rocks in this study are located ~40 m below sea level (the same maximum elevation of the rhyolitic domes). Since Lake Cahuilla has filled to above the elevation that the surface samples in this study were obtained, it is likely that all surface samples in this study were once submerged beneath the surface of Lake Cahuilla and thus have been altered post-emplacement. However, since the hypersaline brines beneath the Salton Sea are partially derived from water from previous and older Lake Cahuilla fill cycles, any alteration to these surface samples from the time of eruption and deposition until present represent a possible stage of alteration from contact with Colorado River flood waters that all rocks in this study have likely undergone (e.g., Sturz, 1989). This alteration process also likely did not leach Li from the volcanic glasses as Li loss from rhyolitic glass takes place at higher temperatures than ambient temperatures (~30°C; Ellis et al., 2022).

All but one of the rocks measured in this study have δ^7Li concentrations that fall within the range of +1.5 - +10.3‰ (the outlier has δ^7Li = -9.1‰). The one outlier will be remeasured for replicability but at this time we have no simple explanation for this measurement. The SSGF brines in this study (δ^7Li = +3.7 - +4.5‰) fall within the same range of lithium isotope compositions as the rocks but are substantially less variable in isotopic composition than the rock hosts of the brines. This is consistent with O and H isotopic data implying that the brine reservoir is convecting and well-mixed (Williams and McKibben, 1989). The δ^7Li compositions of both rocks and brines in this study overlap with a wide variety of geologic settings that include but are not limited to those of upper continental crust (δ^7Li_{avg} = 0.6‰; Penniston-Dorland et al., 2017 and references therein), river waters (δ^7Li = +1 - +44‰; e.g., Penniston-Dorland et al., 2017 and references therein; Zhang et al., 2022 and references therein), and Mid-Ocean Ridge Basalt (δ^7Li_{avg} = 3.4‰; Penniston-Dorland et al., 2017 and references therein). The wide range in geologic settings that overlap with the isotopic composition of Salton Sea rocks and brines necessitates careful quantitative modeling of isotopic fractionation between the brines and the rocks that they are in contact with to identify the source(s) of the Li in Salton Sea brines.

As one of the lightest elements on the periodic table, lithium has a large relative difference in the mass between its two stable isotopes, ^{6}Li and ^{7}Li (~17%), which leads to large fractionations at low temperatures (<250°C; Chan et al., 1994; Penniston-Dorland et al., 2017 and references therein). The fractionation processes relevant to this study include low temperature precipitation of minerals from fluids, low to moderate temperature fluid-rock interactions, and diffusion of Li through a mineral. Generally, the fractionation of Li isotopes during the formation of secondary minerals during fluid-rock interactions occurs because of preferential incorporation of ^{7}Li into lower coordination environments, such as in an aqueous fluid when compared to clay and oxide/hydroxide minerals forming during water-rock interactions (e.g., Penniston-Dorland et al., 2017 and references therein). The extent of this fractionation is inversely proportional to temperature (Chan et al., 1994; Millot et al., 2010) such that as the temperature of the fluid decreases, the difference between δ^7Li of the host fluid and the secondary minerals forming from that same fluid increases. A consequence of this low temperature weathering is the increase in the δ^7Li of river water (δ^7Li_{avg} = 23‰), lake water (δ^7Li_{avg} = 0.6‰), and seawater (δ^7Li_{avg} = 31‰) compared to both the rocks being weathered (e.g., compare the average river water, δ^7Li_{avg} = 23‰, to the average value of the upper continental crust, δ^7Li_{avg} = 0.6‰) and the minerals forming due to weathering (e.g., compare seawater, δ^7Li_{avg} = 31‰ to that of global average seafloor sediment or GLOSS-II, δ^7Li_{avg} = 0.2‰; Penniston-Dorland et al., 2017 and references therein). At higher temperatures (such as those of the hypersaline brines in the SSGF, >250°C), the isotopic fractionation of Li between the fluid and associated minerals is minimized (Chan et al., 1994; Millot et al., 2010; Penniston-Dorland et al., 2017 and references therein). The effects of Li diffusion on the fractionation of Li are complex and the timescales involved are dependent on the identity of the crystallographic site in which Li has been incorporated into a mineral (e.g., Penniston-Dorland et al., 2017 and references therein). For example, in aqueous fluids and silicate melts, ^{6}Li has been documented to diffuse up to 3% faster than ^{7}Li (Penniston-Dorland et al., 2017 and references therein). While evaporation is a process that effects the bulk Li concentration of brine ponds by increasing Li concentrations of residual brine liquids, because Li is not volatile and thus does not leave the liquid reservoir, it does not fractionate the Li isotopic composition of the residual brine liquids (Godfrey et al., 2013) and thus is not likely one of the processes that would affect the composition of Li isotopes in the SSGF.

The sources and processes that contribute to the Li concentrations and isotopic compositions of the SSGF brines are complex, owing to the variety of rocks present beneath the Salton Sea (fig. 2). On geological timescales, the brine is originally emplaced through the flooding of the Salton Trough periodically with Colorado River water to create ancient Lake Cahuilla (see Geologic Setting, above). These ancient lakes would evaporate, causing an increase in Li concentrations in the remaining water (and ultimately generating the brine-nature of the SSGF brines) but result in little change to the δ^7Li composition of these fluids (Godfrey et al., 2013). Then these brines were buried as the pore fluids in sediments with each successive cycle of Lake Cahuilla filling and evaporating. Elevated heat flow related to the bimodal basaltic-rhyolitic volcanism and deeper heat circulation associated with the tectonic setting would allow for water-rock interactions at moderate temperatures (>250°C). It is also possible that some Li from these volcanic systems enters the SSGF brines at any time from ongoing episodes of volcanism in the region (see Geologic Setting, above). Fluid-rock interactions drove the recrystallization of clay minerals in reacting with the hot brines at depth (e.g., Helgeson, 1968; Muffler and White, 1969), which in isolation should lead to minerals with lighter δ^7Li compositions than the brine, which would become progressively heavier as the minerals forming in reaction with the brine preferentially incorporate ^{6}Li into their crystal structure. Minerals forming as a consequence of interaction with these progressively heavier brines in δ^7Li would have heavier δ^7Li than minerals formed at earlier stages of this process. The increased heat from these hydrothermal reactions may release more Li into the brine from the buried sediments and volcanic rocks (Coffey et al., 2021; Ellis et al., 2022). These processes will be quantitatively handled in a future contribution.

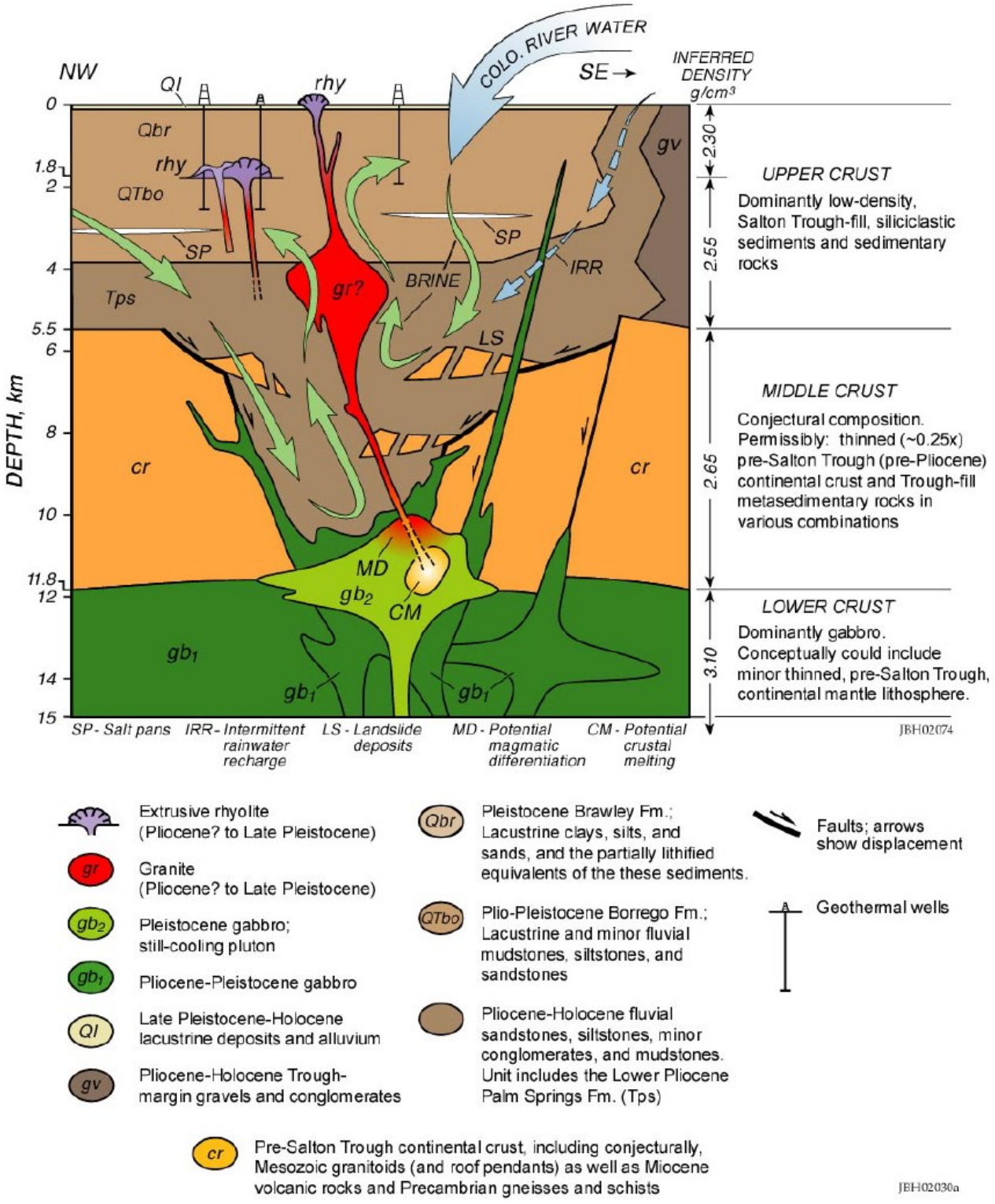

Figure 2: Conceptual model of the SSGF from Hulen et al. (2002).

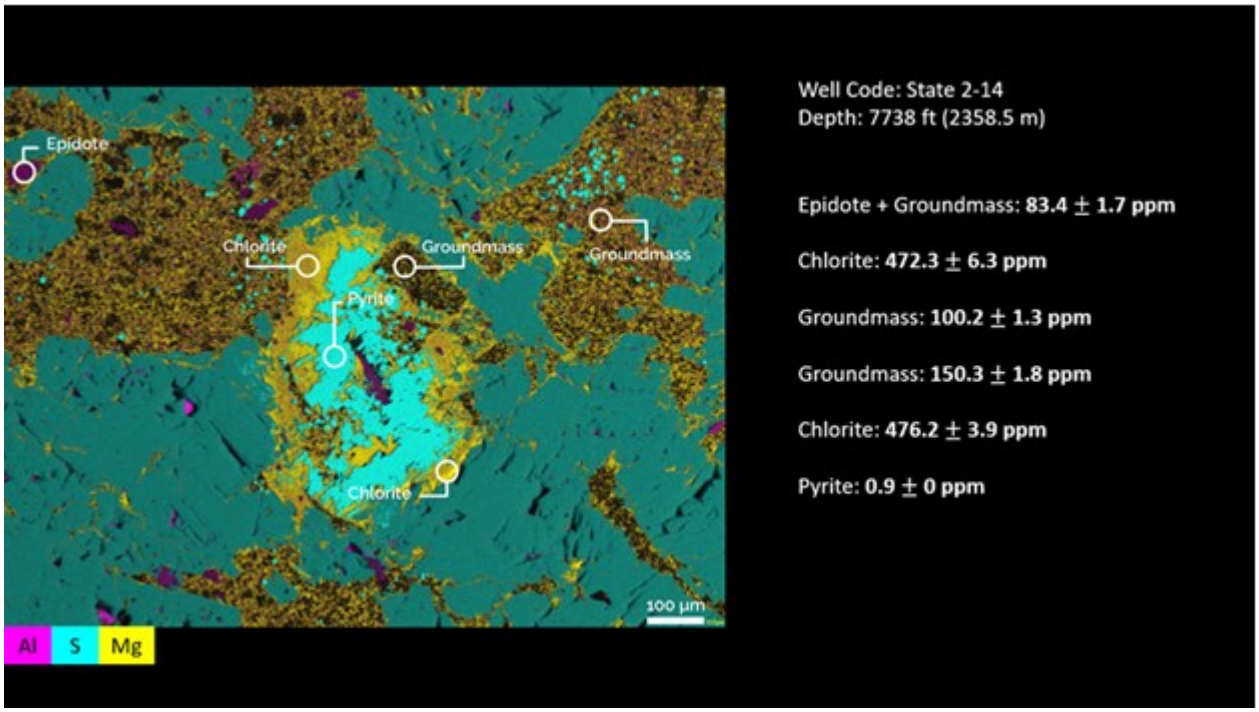

Figure 3: Back Scatter Electron map of metasedimentary anhydrite and mudstone. Relatively aluminum rich regions are represented by magenta, relatively sulfur regions are represented by cyan, and relatively magnesium rich regions are represented by yellow. Anhydrite is the dark cyan mineral that is unlabeled on the sample. Relatively large authigenic chlorite surrounds pyrite.

The highest Li concentrations are measured in chlorites from the calcite-chlorite metamorphic zone (McDowell and Elders, 1980). Chlorite-rich groundmasses in these same metasedimentary rocks are also elevated relative to non-chlorite bearing groundmass measurements. In the calcite-chlorite zone, chlorites are observed surrounding larger clasts of epidote, pyrite, and anhydrite. The largest chlorites are found around anhedral, poikiloblastic pyrite clasts. The spatial relationship between pyrite and chlorite indicates that chlorite is forming as the pyrite is broken down (fig. 3). The chloritization of pyrite is not the only way in which chlorite is formed in the calcite-chlorite zone. Previous studies on rocks in the Salton Trough have noted the appearance of chlorite coincides with the disappearance of kaolinite, ankerite, dolomite, calcite, and quartz (Cho et al., 1988; Muffler and White, 1969) and that chlorite has been observed as replacing plagioclase in thin sections (McDowell and Elders, 1980). The high Li concentration of chlorite in these rocks (269-581 ppm) along with overlapping δ^7Li values of these rocks (δ^7Li = +2.0 - +4.3‰) with the SSGF brines (δ^7Li = +3.7 - +4.7‰) suggest that chlorite is incorporating Li from the brine into its crystal structure because of the small degree of Li isotopic fractionation expected at temperatures >250°C (Chan et al., 1994; Penniston-Dorland et al., 2017 and references therein). Chlorites from the biotite metamorphic zone contain less Li than their calcite-chlorite zone counterparts (up to 104 ppm) but their host rocks also overlap with δ^7Li values of the SSGF brine (δ^7Li = +4.3 - +5.1‰ in the host rock). Not all metasedimentary rocks in the SSGF overlap with the δ^7Li values of the SSGF brine. Epidotized mudstone from the biotite metamorphic zone has a range in δ^7Li values from 6.2-7.9‰. This indicates that either only rocks that incorporate large amounts of Li through metamorphic reactions reflect the brine composition with respect to Li isotopes, the partitioning of Li between the epidotized mudstone and the brine favors heavier lithium over lighter lithium (possibly as a consequence of release of adsorbed – lighter – Li from the minerals of these rocks at higher temperatures; e.g., Coffey et al., 2021), or that brine chemistry has a minimal effect on the lithium isotopes recorded by the metasedimentary rocks and any overlap between the brine values and the rock values is circumstantial. Future work will quantitatively investigate these possibilities. We conclude broadly that because chlorite is a metamorphic mineral, incorporates relatively large amounts of Li in it, and the host rocks for the chlorite overlap in δ^7Li values with the SSGF brine, it is likely that the δ^7Li composition of the host rock and brine reflects hydrothermal interactions between the two at depth.

6. CONCLUSIONS

All the rocks in this study have been in contact with brines from the SSGF, from the surface rocks that were in contact with the surface brine as Lake Cahuilla evaporated or the geothermal brine at depth; however, since Lake Cahuilla would have had surface temperature waters and most buried rocks would have been in contact with Lake Cahuilla waters prior to burial, the surface rocks are still a good analog for the Li concentrations and Li isotopic compositions prior to burial. The overlap in δ^7Li values between Salton Sea brines and rocks with various Li sources, including other brines, indicates that contact with sedimentary, metasedimentary, and igneous rocks within the Salton Trough have likely all contributed to the chemical characteristics of the current brine. Quantitative handling of the isotopic data will be used in a future contribution to demonstrate the exact source(s) of Li in the SSGF brines and reservoir rocks. As for what happens

to the Li at depth, chlorite in the calcite-chlorite zone likely incorporates Li from the SSGF brine waters, acting as a Li sink, as it forms due to hydrothermal metamorphic reactions. Coupled process geochemical modeling is being conducted to evaluate likely fluid-mineral interactions, and to predict whether the lithium-bearing mineral phases in the geothermal reservoir may recharge lithium to the brine as lithium is recovered from the geothermal brines at the surface and lithium-poor brines are reinjected back into the reservoir. This may help guide future reinjection strategies to help sustain lithium production and maximize lithium recovery from this resource.

ACKNOWLEDGMENTS

We thank Berkshire Hathaway Energy Renewables/CalEnergy and Controlled Thermal Resources for kindly providing access to many of the rock and brine samples that were analyzed in this study. We also thank Patrick Muffler (USGS) for sharing the results of his past studies of the Salton Sea geothermal field with our team. This work is supported by the U.S. Department of Energy, Office of Energy Efficiency and Renewable Energy (EERE), Geothermal Technologies Office, under Award Number DE-AC02–05CH11231 with Lawrence Berkeley National Laboratory.

REFERENCES

Ambrose, H., Kendall, A., 2020. Understanding the future of lithium: Part 1, resource model. Journal of Industrial Ecology 24, 80–89. https://doi.org/10.1111/jiec.12949

Araoka, D., Kawahata, H., Takagi, T., Watanabe, Y., Nishimura, K., Nishio, Y., 2014. Lithium and strontium isotopic systematics in playas in Nevada, USA: constraints on the origin of lithium. Miner Deposita 49, 371–379. https://doi.org/10.1007/s00126-013-0495-y

Babcock, E.A., 1974. Geology of the Northeast Margin of the Salton Trough, Salton Sea, California. Geol Soc America Bull 85, 321. https://doi.org/10.1130/0016-7606(1974)85<321:GOTNMO>2.0.CO;2

Chan, L.-H., Gieskes, J.M., Chen-Feng, Y., Edmond, J.M., 1994. Lithium isotope geochemistry of sediments and hydrothermal fluids of the Guaymas Basin, Gulf of California. Geochimica et Cosmochimica Acta 58, 4443–4454. https://doi.org/10.1016/0016-7037(94)90346-8

Cho, M., Liou, J.G., Bird, D.K., 1988. Prograde Phase Relations in the State 2-14 Well Metasandstones, Salton Sea Geothermal Field, California. J. Geophys. Res. 93, 13081–13103. https://doi.org/10.1029/JB093iB11p13081

Chordia, M., Wickerts, S., Nordelöf, A., Arvidsson, R., 2022. Life cycle environmental impacts of current and future battery-grade lithium supply from brine and spodumene. Resources, Conservation and Recycling 187, 106634. https://doi.org/10.1016/j.resconrec.2022.106634

Coffey, D.M., Munk, L.A., Ibarra, D.E., Butler, K.L., Boutt, D.F., Jenckes, J., 2021. Lithium Storage and Release From Lacustrine Sediments: Implications for Lithium Enrichment and Sustainability in Continental Brines. Geochem Geophys Geosyst 22. https://doi.org/10.1029/2021GC009916

Coplen, T., 1976. Cooperative geochemical resource assessment of the Mesa Geothermal system. Final Report California Univ.

Elders, W.A., Rex, R.W., Robinson, P.T., Biehler, S., Meidav, T., 1972. Crustal Spreading in Southern California: The Imperial Valley and the Gulf of California formed by the rifting apart of a continental plate. Science 178, 15–24.

Elders, W.A., Sass, J.H., 1988. THE SALTON SEA SCIENTIFIC DRILLING PROJECT. J. Geophys. Res. 93, 12953–12968. https://doi.org/10.1029/JB093iB11p12953

Ellis, B.S., Szymanowski, D., Harris, C., Tollan, P.M.E., Neukampf, J., Guillong, M., Cortes-Calderon, E.A., Bachmann, O., 2022. Evaluating the Potential of Rhyolitic Glass as a Lithium Source for Brine Deposits. Economic Geology 117, 91–105. https://doi.org/10.5382/econgeo.4866

Garcia, M.G., Borda, L.G., Godfrey, L.V., López Steinmetz, R.L., Losada-Calderon, A., 2020. Characterization of lithium cycling in the Salar De Olaroz, Central Andes, using a geochemical and isotopic approach. Chemical Geology 531, 119340. https://doi.org/10.1016/j.chemgeo.2019.119340

Godfrey, L., Álvarez-Amado, F., 2020. Volcanic and Saline Lithium Inputs to the Salar de Atacama. Minerals 10, 201. https://doi.org/10.3390/min10020201

Godfrey, L.V., Chan, L.-H., Alonso, R.N., Lowenstein, T.K., McDonough, W.F., Houston, J., Li, J., Bobst, A., Jordan, T.E., 2013. The role of climate in the accumulation of lithium-rich brine in the Central Andes. Applied Geochemistry 38, 92–102. https://doi.org/10.1016/j.apgeochem.2013.09.002

Gratuze, B., 1999. Obsidian Characterization by Laser Ablation ICP-MS and its Application to Prehistoric Trade in the Mediterranean and the Near East: Sources and Distribution of Obsidian within the Aegean and Anatolia. Journal of Archaeological Science 26, 869–881. https://doi.org/10.1006/jasc.1999.0459

Han, L., Hole, J.A., Stock, J.M., Fuis, G.S., Kell, A., Driscoll, N.W., Kent, G.M., Harding, A.J., Rymer, M.J., González-Fernández, A., Lázaro-Mancilla, O., 2016. Continental rupture and the creation of new crust in the Salton Trough rift, Southern California and northern Mexico: Results from the Salton Seismic Imaging Project. J. Geophys. Res. Solid Earth 121, 7469–7489. https://doi.org/10.1002/2016JB013139

He, M.-Y., Luo, C.-G., Yang, H.-J., Kong, F.-C., Li, Y.-L., Deng, L., Zhang, X.-Y., Yang, K.-Y., 2020. Sources and a proposal for comprehensive exploitation of lithium brine deposits in the Qaidam Basin on the northern Tibetan Plateau, China: Evidence from Li isotopes. Ore Geology Reviews 117, 103277. https://doi.org/10.1016/j.oregeorev.2019.103277

Helgeson, H.C., 1968. Geologic and thermodynamic characteristics of the Salton Sea geothermal system. American Journal of Science 266, 129–166.

Herzig, C.T., Elders, W.A., 1988. NATURE AND SIGNIFICANCE OF IGNEOUS ROCKS CORED IN THE STATE 2-14 RESEARCH BOREHOLE: SALTON SEA SCIENTIFIC DRILLING PROJECT, CALIFORNIA. J. Geophys. Res. 93, 13069–13080. https://doi.org/10.1029/JB093iB11p13069

Herzig, C.T., Jacobs, D.C., 1994. Cenozoic volcanism and two-stage extension in the Salton trough, southern California and northern Baja California. Geol 22, 991. https://doi.org/10.1130/0091-7613(1994)022<0991:CVATSE>2.3.CO;2

Herzig, C.T., Mehegan, J.M., Stelting, C.E., 1988. Lithostratigraphy of the State 2-14 Borehole: Salton Sea Scientific Drilling Project. J. Geophys. Res. 93, 12969–12980. https://doi.org/10.1029/JB093iB11p12969

Hulen, J.B., Kaspereit, D., Norton, D.L., Osborn, W., Pulka, F.S., 2002. Refined conceptual modeling and a new resource estimate for the Salton Sea geothermal field, Imperial Valley, California. Geothermal Resources Council Transactions 26, 29–36.

Jaskula, B., 2022. Lithium, Mineral Commodity Summaries. United States Geological Survey.

Jochum, K.P., Dingwell, D.B., Rocholl, A., Stoll, B., Hofmann, A.W., Becker, S., Besmehn, A., Bessette, D., Dietze, H.-J., Dulski, P., Erzinger, J., Hellebrand, E., Hoppe, P., Horn, I., Janssens, K., Jenner, G.A., Klein, M., McDonough, W.F., Maetz, M., Mezger, K., Müker, C., Nikogosian, I.K., Pickhardt, C., Raczek, I., Rhede, D., Seufert, H.M., Simakin, S.G., Sobolev, A.V., Spettel, B., Straub, S., Vincze, L., Wallianos, A., Weckwerth, G., Weyer, S., Wolf, D., Zimmer, M., 2000. The Preparation and Preliminary Characterisation of Eight Geological MPI-DING Reference Glasses for In-Situ Microanalysis. Geostandards and Geoanalytical Research 24, 87–133. https://doi.org/10.1111/j.1751-908X.2000.tb00590.x

Kalderon-Asael, B., Katchinoff, J.A., Planavsky, N.J., Hood, A.V.S., Dellinger, M., Bellefroid, E.J., Jones, D.S., Hofmann, A., Ossa, F.O., Macdonald, F.A. and Wang, C., 2021. A lithium-isotope perspective on the evolution of carbon and silicon cycles. *Nature*, *595*(7867), 394-398. https://doi.org/10.1038/s41586-021-03612-1

Kelley, K.A., Plank, T., Ludden, J., Staudigel, H., 2003. Composition of altered oceanic crust at ODP Sites 801 and 1149: ALTERED OCEANIC CRUST. Geochem. Geophys. Geosyst. 4, n/a-n/a. https://doi.org/10.1029/2002GC000435

Kelly, J.C., Wang, M., Dai, Q., Winjobi, O., 2021. Energy, greenhouse gas, and water life cycle analysis of lithium carbonate and lithium hydroxide monohydrate from brine and ore resources and their use in lithium ion battery cathodes and lithium ion batteries. Resources, Conservation and Recycling 174, 105762. https://doi.org/10.1016/j.resconrec.2021.105762

Liu, W., Agusdinata, D.B., 2020. Interdependencies of lithium mining and communities sustainability in Salar de Atacama, Chile. Journal of Cleaner Production 260, 120838. https://doi.org/10.1016/j.jclepro.2020.120838

Maimoni, A., 1982. Minerals recovery from salton sea geothermal brines: a literature review and proposed cementation process. Geothermics 11, 239–258. https://doi.org/10.1016/0375-6505(82)90031-1

Mark, D.F., Renne, P.R., Dymock, R.C., Smith, V.C., Simon, J.I., Morgan, L.E., Staff, R.A., Ellis, B.S., Pearce, N.J.G., 2017. High-precision $^{40}Ar/^{39}Ar$ dating of Pleistocene tuffs and temporal anchoring of the Matuyama-Brunhes boundary. Quaternary Geochronolgy, 39, 1-23, https://doi.org/10.1016/j.quageo.2017.01.002

Matti, J.C., Morton, D.M., Cox, B.F., 1985. Distribution and geologic relations of fault systems in the vicinity of the central Transverse Ranges, southern California (No. 2331–1258). US Geological Survey.

McDowell, S.D., Elders, W.A., 1980. Authigenic layer silicate minerals in borehole Elmore 1, Salton Sea Geothermal Field, California, USA. Contr. Mineral. and Petrol. 74, 293–310. https://doi.org/10.1007/BF00371699

McKibben, M.A., Elders, W.A., Raju, A.S.K., 2021. Lithium and Other Geothermal Mineral and Energy Resources Beneath the Salton Sea. Crisis at the Salton Sea: Research Gaps and Opportunities 16.

McKibben, M. A., Williams, A. E., Okubo, S. (1988a) Metamorphosed Plio-Pleistocene evaporites and the origins of hypersaline brines in the Salton Sea geothermal system, California: fluid inclusion evidence. *Geochimica et Cosmochimica Acta*, Vol. 52, pp. 1047-1056.

McKibben, M. A., Andes, J. P., Jr., Williams, A. E., (1988b) Active ore-formation at a brine interface in metamorphosed deltaic-lacustrine sediments: the Salton Sea geothermal system, California. *Economic Geology*, Vol. 83, pp. 511-523.Millot, R., Scaillet, B., Sanjuan, B., 2010. Lithium isotopes in island arc geothermal systems: Guadeloupe, Martinique (French West Indies) and experimental approach. Geochimica et Cosmochimica Acta 74, 1852–1871. https://doi.org/10.1016/j.gca.2009.12.007

Merriam, R. and Bischoff, J.L., 1975. Bishop ash; a widespread volcanic ash extended to southern California. Journal of Sedimentary Research, 45(1), pp.207-211. https://doi.org/10.1306/212F6D07-2B24-11D7-8648000102C1865D

Muffler, L.P., White, D.E., 1969. Active metamorphism of upper Cenozoic sediments in the Salton Sea geothermal field and the Salton Trough, southeastern California. Geological Society of America Bulletin 80, 157–181.

Munk, L.A., Boutt, D.F., Hynek, S.A., Moran, B.J., 2018. Hydrogeochemical fluxes and processes contributing to the formation of lithium-enriched brines in a hyper-arid continental basin. Chemical Geology 493, 37–57. https://doi.org/10.1016/j.chemgeo.2018.05.013

Olivetti, E.A., Ceder, G., Gaustad, G.G., Fu, X., 2017. Lithium-Ion Battery Supply Chain Considerations: Analysis of Potential Bottlenecks in Critical Metals. Joule 1, 229–243. https://doi.org/10.1016/j.joule.2017.08.019

Penniston-Dorland, S., Liu, X.-M., Rudnick, R.L., 2017. Lithium Isotope Geochemistry. Reviews in Mineralogy and Geochemistry 82, 165–217. https://doi.org/10.2138/rmg.2017.82.6

Robinson, P.T., Elders, W.A., Muffler, L.J.P., 1976. Quaternary volcanism in the Salton Sea geothermal field, Imperial Valley, California. Geol Soc America Bull 87, 347. https://doi.org/10.1130/0016-7606(1976)87<347:QVITSS>2.0.CO;2

Rockwell, T.K., Meltzner, A.J., Haaker, E.C., Madugo, D., 2022. The late Holocene history of Lake Cahuilla: Two thousand years of repeated fillings within the Salton Trough, Imperial Valley, California. Quaternary Science Reviews 282, 107456. https://doi.org/10.1016/j.quascirev.2022.107456

Sanjuan, B., Millot, R., Innocent, Ch., Dezayes, Ch., Scheiber, J., Brach, M., 2016. Major geochemical characteristics of geothermal brines from the Upper Rhine Graben granitic basement with constraints on temperature and circulation. Chemical Geology 428, 27–47. https://doi.org/10.1016/j.chemgeo.2016.02.021

Sarna-Wojcicki, A.M., Bowman, H.R., Meyer, C.E., Russell, P.C., Woodward, M.J., McCoy, G., Rowe Jr, J.J., Baedecker, P.A., Asaro, F. and Michael, H., 1984. Chemical analyses, correlations, and ages of upper Pliocene and Pleistocene ash layers of east-central and southern California (No. 1293). https://doi.org/10.3133/pp1293

Schmitt, A.K., Hulen, J.B., 2008. Buried rhyolites within the active, high-temperature Salton Sea geothermal system. Journal of Volcanology and Geothermal Research 178, 708–718. https://doi.org/10.1016/j.jvolgeores.2008.09.001

Schmitt, A.K., Perrine, A.R., Rhodes, E.J., Fischer, C., 2019. Age of Obsidian Butte in Imperial County, California, Through Infrared Stimulated Luminescence Dating of Potassium Feldspar from Tuffaceous Sediment. California Archaeology 11, 5–20. https://doi.org/10.1080/1947461X.2019.1581678

Skinner, B.J., White, D.E., Rose, H.J., Mays, R.E., 1967. Sulfides associated with the Salton Sea geothermal brine. Economic Geology 62, 316–330. https://doi.org/10.2113/gsecongeo.62.3.316

Stock, J., Hodges, K., 1989. Pre-Pliocene extension around the Gulf of California and the transfer of Baja California to the Pacific plate. Tectonics 8, 99–115.

Sturz, A., 1989. Low-temperature hydrothermal alteration in near-surface sediments, Salton Sea Geothermal Area. J. Geophys. Res. 94, 4015–4024. https://doi.org/10.1029/JB094iB04p04015

Sun, X., Hao, H., Zhao, F., Liu, Z., 2017. Tracing global lithium flow: A trade-linked material flow analysis. Resources, Conservation and Recycling 124, 50–61. https://doi.org/10.1016/j.resconrec.2017.04.012

Tompson, A.F.B., 2016. Born from a flood: The Salton Sea and its story of survival. J. Earth Sci. 27, 89–97. https://doi.org/10.1007/s12583-016-0630-7

U.S.G.S., 2022. U.S. Geological Survey releases 2022 list of critical minerals. U.S.G.S.

Williams, A.E., McKibben, M.A., 1989. A brine interface in the Salton Sea Geothermal System, California: Fluid geochemical and isotopic characteristics. Geochimica et Cosmochimica Acta 53, 1905–1920. https://doi.org/10.1016/0016-7037(89)90312-8

Winker, C.D., Kidwell, S.M., 1986. Paleocurrent evidence for lateral displacement of the Pliocene Colorado River delta by the San Andreas fault system, southeastern California. Geol 14, 788. https://doi.org/10.1130/0091-7613(1986)14<788:PEFLDO>2.0.CO;2

Wright, H.M., Vazquez, J.A., Champion, D.E., Calvert, A.T., Mangan, M.T., Stelten, M., Cooper, K.M., Herzig, C., Schriener, A., 2015. Episodic Holocene eruption of the Salton Buttes rhyolites, California, from paleomagnetic, U-Th, and Ar/Ar dating: Salton Buttes rhyolites. Geochem. Geophys. Geosyst. 16, 1198–1210. https://doi.org/10.1002/2015GC005714

Zhang, F., Dellinger, M., Hilton, R.G., Yu, J., Allen, M.B., Densmore, A.L., Sun, H., Jin, Z., 2022. Hydrological control of river and seawater lithium isotopes. Nat Commun 13, 3359. https://doi.org/10.1038/s41467-022-31076-y